ROTORCRAFT AERODYNAMIC AND AEROACOUSTIC MODELLING USING VORTEX PARTICLE METHODS

Daniel G. Opoku[(1)], Dimitris G. Triantos[(2)], Fred Nitzsche[(1)], Spyros G. Voutsinas[(2)]
[(1)]Carleton University, Ottawa, Canada, [(2)]National Technical University of Athens, Greece

Keywords: *Rotorcraft Aerodynamics, Rotorcraft Aeroacoustics, and Vortex Particle Methods*

Abstract

The initial development of a combined active aeroelastic aeroacoustic rotorcraft code is discussed. The GENeral Unsteady Vortex Particle code (GENUVP) is used as the aerodynamic component of the combined code. A brief discussion of the theory behind GENUVP's use of an unsteady panel method with a vortex particle wake is presented. Modifications to GENUVP to increase its computational efficiency are discussed. The implementation of a new aeroacoustic component in GENUVP is summarized. An overview of the combined active aeroelastic aeroacoustic code under development is presented. Results from the current work, including aerodynamic modelling of the NASA/ARMY/MIT Active Twist Rotor (ATR) and acoustic modelling of a NASA scale UH1H rotor are presented.

1 Introduction

Computational modelling of rotorcraft aerodynamics is a unique and challenging problem. To properly model a rotorcraft, the interaction between several bodies must be captured. In addition, the influence of the wake must be accounted for as it has strong influence on the aerodynamics of the rotor. These factors combine to make rotorcraft modelling a difficult and computationally expensive task.

Accurate modelling of rotorcraft aerodynamics is essential for research and development in several other disciplines. Structural dynamic and aeroelastic analysis of rotor blades requires an aerodynamic model capable of accurately predicting loads to determine the interaction between the structure and aerodynamics. Prediction of noise also requires accurate aerodynamic input to capture phenomena such as blade-vortex interaction (BVI). Investigation of methods for active and passive control for vibration and noise reduction also requires accurate aerodynamic models to predict the response that must be controlled.

Grid based computational fluids dynamics (CFD) codes have been used with varied success to model rotorcraft aerodynamics [1] - [3]. While CFD has the potential to eventually provide very detailed aerodynamic calculations, it often has difficulty in capturing wake effects. In addition, CFD is generally too computationally expensive to closely couple with analyses for other studies, such as aeroelasticity. An alternative approach is to use a panel method or lifting-line model coupled with a vortex wake model for aerodynamic modelling [4] - [6]. These methods have been shown to accurately model the aerodynamics of a rotor in a variety of flight situations with computational costs that are orders of magnitude less than CFD [7].

The GENeral Unsteady Vortex Particle (GENUVP) code was developed at the National Technical University of Athens (NTUA) by Voutsinas et al. [8] [9]. GENUVP is a panel method code with a vortex particle wake model for calculating the flowfield around multi-component configurations. Initial use of GENUVP focused on the modelling of wind-turbines. Voutsinas and Triantos then extended the application of GENUVP to modelling of rotorcraft aerodynamics and aeroacoustics, while also adding features to reduce its computational cost [10] [11].

The broad objective of the current work is to develop a combined active aeroelastic aeroacoustic rotorcraft code. Through collaboration with NTUA, GENUVP will be used by Carleton University as the aerodynamic component of the combined code. One of the first applications of the combined code will be aeroelastic and aeroacoustic modelling of the NASA/ARMY/MIT Active Twist Rotor (ATR) [12]. This paper focuses on the first stage of this work, which involves using GENUVP for aerodynamic modelling of the ATR, and validation of a new acoustic component that was added to GENUVP.

2 Aerodynamic formulation

Voutsinas et al. [8] - [11] give details of GENUVP's aerodynamic formulation. Only the main aspects of the formulation will be repeated here for completeness.

2.1 Helmholtz decomposition

The core theory of GENUVP is the use of the Helmholtz decomposition theorem through which the influence of solid bodies such as rotor blades, fuselage, and stabilizers is captured along with the influence of the wake. Consider the unsteady flow of an incompressible and inviscid fluid around a multi-component configuration. The bodies are allowed to move independently, a necessary feature for helicopter configurations. Let $\vec{u}(\vec{x};t), \vec{x} \in D, t \geq 0$ denote the velocity of the fluid where D is the flow field. Then according to the Helmholtz decomposition theorem, $\vec{u}$ can be split in two parts: an irrotational and a rotational one. Usually the presence of solid boundaries is included in the irrotational part $\vec{u}_{solid}$ whereas the wakes are, as expected, included in the rotational part $\vec{u}_{wake}$. So,

$$\vec{u}(\vec{x};t) = \vec{u}_{ext}(\vec{x};t) + \vec{u}_{solid}(\vec{x};t) + \vec{u}_{wake}(\vec{x};t) \qquad (1)$$

where $\vec{u}_{ext}$ denotes a given external field possibly varying in space and time. Green's theorem provides the means to express $\vec{u}_{solid}$ through surface singularity distributions suggesting the use of a panel method in approximating this term. As for $\vec{u}_{wake}$, the Biot-Savart law gives,

$$\vec{u}_{wake}(\vec{x}_o;t) = \int_{D_\omega(t)} \frac{\vec{\omega}(\vec{x};t) \times (\vec{x}_o - \vec{x})}{4\pi |\vec{x}_o - \vec{x}|^3} dD \qquad (2)$$

where $D_\omega(t)$ denotes the support of vorticity. From (2), the use of vortex methods (VMs) in approximating $\vec{u}_{wake}$ is straightforward. So decomposition (1) implies as a suitable numerical model the combination of a panel method with VMs. The two parts in (1) must be linked to each other through appropriate conditions, which will feed $\vec{u}_{wake}$ with vorticity continuously in time.

2.2 Panel method - u_{SOLID}

Following Hess [13], an indirect panel method is used for modeling solid bodies in GENUVP. In GENUVP, lifting bodies, i.e. the rotor blades or stabilizers, can be modelled as either thin or thick lifting bodies. Thin lifting bodies are modelled using dipole distributions and thick lifting bodies are modelled using a combination of dipole and source distributions. For the current work, thin lifting bodies were used for modelling the rotor blades. In GENUVP, trailing and tip edge wake strips are emitted at every time step – referred to as the near-wake. Matching the strength of each wake element with the strength of the adjacent emitting dipole element (i.e. trailing or tip edge) on the blade enforces a zero pressure jump Kutta condition.

Non-lifting bodies can also be modelled in GENUVP using source distributions to model the body geometry. In this way, the effects of a fuselage on the rotor inflow can be modelled.

2.3 Vortex particle methods – u_{WAKE}

It is a well-established fact that the wake has a large influence on the aerodynamics of rotorcraft [7]. As such, an accurate wake model is essential for rotorcraft aerodynamic modelling. Following Rehbach [14], a vortex

"blob" approach was taken to modelling the far-field wake in GENUVP. With this approach the wake is represented by a cloud of vortex particles, each with associated vector quantities of intensity, velocity, and position. The evolution of the vortex particle wake is carried out using a Lagrangian description that accounts for the "stretching" of vorticity. Modelling of vortex stretching allows the vortex particle wake to capture the effects of wake deformation. The induced velocity due to each vortex particle is determined with a smoothed approximation of the Biot-Savart law given by Beale and Majda [15].

2.4 Near to far field coupling scheme

After the panel method calculations of a given time step, the near-wake strip elements are transformed into vortex particles and become a part of the far-wake. This is done by integrating [8] the vorticity of each near-wake dipole element to form a vortex particle. The new vortex particles become a part of the far wake, which evolves prior to the next time step. Refer to Figure 1.

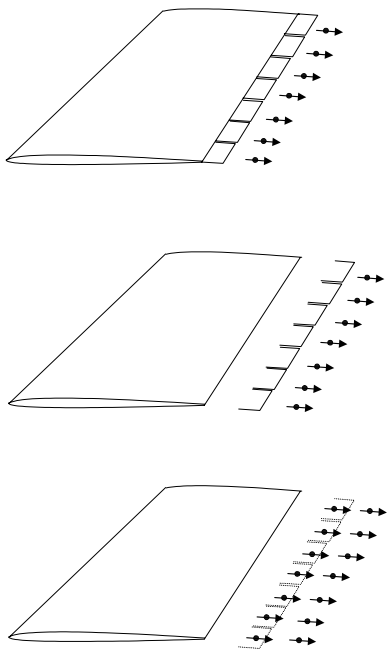

Figure 1 A picture of the formation of vortex particles from a trailing edge wake strip.

2.5 Reduction of computational cost

For an effective code, computational cost must be kept manageable. Two schemes were introduced into GENUVP to reduce the code's computational cost – subgrid and particle-mesh approximations [10] [11].

Subgrid approximations were implemented to help reduce the cost of the panel method calculations. As pointed out early by Hess [16], exact integral evaluations are necessary only when the distance between control point and the panel center is small. In fact when the distance of the evaluation point from the panel gets bigger than 4 times the maximum diagonal of the panel, the integral evaluation can be reduced to a point calculation. Reversing this result, one can expect that the error will be also small if distant panels are grouped into larger ones over which the integrals are evaluated [17]. A strategy to such a grouping has been extended to dipole distributions and implemented [11] by introducing a sequence of panelling at different levels of refinement as shown in Figure 2. Calculations start at the lowest level (coarse panelling). Depending on the distance between the panel center and the evaluation point, the calculations will either proceed with the integral evaluation over the large panel or pass to the next and more refined level of panelling as shown in Figure 2. Consider a panel of surface S, which contains n panels of the highest level in which the unknown singularity X is defined. Let I_1 denote the value of the integral evaluated over S for unitary singularity strength. Then the collective contribution of the n panels is approximated by:

$$I = \sum_{i=1}^{n} I_1 \frac{S_i}{S} X_i \qquad (3)$$

where S_i denotes the surface area of the i-th high-level panel. Depending on the number of unknowns the final system is either solved directly or iteratively in which case the matrix need not be stored. Thus panelling of the order of several thousands can be used even on ordinary workstations.

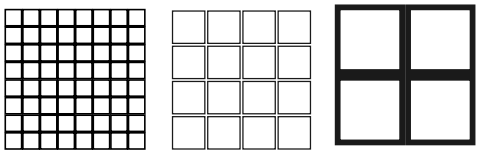

(a) The three levels of paneling

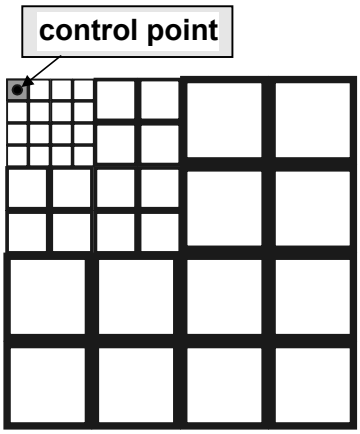

(b) The activation of the different levels

Figure 2 A diagram of the grid refinement levels used for subgrid approximation.

Conventional vortex methods involve direct evaluation of the velocity and the deformation at every blob position based on the Biot-Savart law. This means that for N vortex blobs a complete time step requires N^2 point-to-point calculations. In engineering applications N will increase continuously in time and so the computational cost will grow exponentially leading at large times to prohibitive levels. One way of having reasonable cost is the use of Particle-Mesh (PM) techniques [18], which reduces the cost to $N.logN$ calculations. The concept is simple: For a large number of blobs, $\vec{u}$ and its spatial derivatives defining the deformation tensor $\vec{D}$, are evaluated at the nodes of a Cartesian grid containing $D_\omega(t)$. Then local interpolation is used to determine $\vec{u}$ and $\vec{D}$ at the exact positions of the blobs. To this end, the vector potential $\vec{A}$ of $\vec{u}_{wake}$ is introduced: $\nabla \times \vec{u}_{wake} = \vec{A}$ and the corresponding Poisson equation:

$$\nabla^2 \vec{A} = -\vec{\omega}, in D_\omega \qquad (4)$$

is solved by means of a Fourier type method. This choice has been made in order to keep the cost to a minimum. More specifically at every time step the PM calculation procedure involves the following steps:

The projection step.

Vorticity is evaluated over a Cartesian mesh that includes all vortex blobs, by projecting the intensity of the vortex blobs located within a cell of the mesh to the vertices of the cell:

$$\vec{\omega}_{i,j,k} = \frac{1}{\delta D} \sum_m \vec{\Omega}_m \zeta(\vec{x}_{i,j,k} - \vec{Z}_m) \qquad (5)$$

where $\vec{\omega}_{i,j,k}$ is the nodal vorticity, $\vec{x}_{i,j,k}$ is the position of node (i,j,k), δD is the volume of the grid cell, and $\zeta(.)$ is the projection function.

The solution step.

Equation (4) is discretized with standard central differences leading to three heptadiagonal linear systems,

$$\frac{\vec{A}_{i+1,j,k} - 2\vec{A}_{i,j,k} + \vec{A}_{i-1,j,k}}{\Delta x^2} + \frac{\vec{A}_{i,j+1,k} - 2\vec{A}_{i,j,k} + \vec{A}_{i,j-1,k}}{\Delta y^2} + \frac{\vec{A}_{i,j,k+1} - 2\vec{A}_{i,j,k} + \vec{A}_{i,j,k-1}}{\Delta z^2} = -\vec{\omega}_{i,j,k} \qquad (6)$$

The values of $\vec{A}$ at the boundary nodes of the grid are provided by point-to-point Biot-Savart calculations. To solve (6) first a two-dimensional Fourier transform is performed resulting in tri-diagonal linear systems. Then the Thomas algorithm is applied. Finally a reverse two-dimensional Fourier transform follows, which provides the nodal values of $\vec{A}$. Once the nodal values of the vector potential are obtained, standard central differences are used to evaluate the velocity $\nabla \times \vec{A}$ and the deformation $\vec{d} = (\vec{\omega}\nabla)\vec{u}$ at the nodes of the grid.

The interpolation step.

The velocity and the deformation of vorticity of each vortex blob are calculated by means of the same procedure used for interpolating the nodal values of vorticity as

follows:

$$\vec{u}_m = \sum_m \vec{u}_{i,j,k}\zeta(\vec{Z}_m - \vec{x}_{i,j,k}) \quad (7a)$$

$$\frac{d\vec{\Omega}_m}{dt} = \vec{d}_m = \sum_m \vec{d}_{i,j,k}\zeta(\vec{Z}_m - \vec{x}_{i,j,k}) \quad (7b)$$

where $\vec{u}_m$ and $\vec{d}_m$ denote the velocity and rate of deformation of the nth vortex blob, whereas $\vec{u}_{i,j,k}$ and $\vec{d}_{i,j,k}$ denote the velocity and rate of deformation at grid node i,j,k. Summation in (7) runs over the neighbouring nodes according to the interpolation scheme.

Accuracy in PM methods is restricted by the cell size. In order to reduce the error of PM schemes, local corrections proposed by Anderson [19] are introduced. Experience has shown that even corrected PM schemes are not sufficiently accurate and therefore they should not be applied to areas of major importance. In GENUVP a mixed scheme has been followed which excludes areas close to solid boundaries from the PM calculations. In these areas the Biot-Savart law is used. For example in the case of forward-flight, the PM region starts downstream of the tail rotor and extends to infinity.

3 Acoustic formulation

Regarding rotorcraft aeroacoustic modelling, the most widely used formulation is based on the Ffowcs Williams-Hawkings (FW-H) equation [20]. Let $\boldsymbol{x}$ and $\boldsymbol{y}$ be the observer and source position vectors respectively, and $f(\boldsymbol{y},t) = 0$ describe the motion of the surface of a body.

$$\left(\frac{1}{c^2}\frac{\partial^2}{\partial t^2} - \nabla^2\right)p' = \frac{\partial}{\partial t}\left[\rho_o v_n |\nabla f|\delta(f)\right] - \frac{\partial}{\partial x_i}\left[l_i|\nabla f|\delta(f)\right] + \frac{\partial^2}{\partial x_i \partial x_j}\left[T_{ij}H(f)\right] \quad (8)$$

The FW-H equation (8) gives the sound generated by the body moving through a fluid, where p', is the acoustic pressure at the observer position, c and ρ_o are the speed of sound and the density of the undisturbed medium respectively, $v_n = v_i n_i$ is the local normal velocity on the body surface (n_i is the body local outward normal), l_i is the local force on the fluid per unit area, and T_{ij} is the Lighthill stress tensor. $\delta(f)$ and $H(f)$ are the Dirac delta and Heaviside function respectively. The three terms on the right-hand side of (8) are the thickness, loading, and quadrupole noise sources, respectively. The thickness noise source accounts for noise due to the displacement of the fluid by the finite thickness of the body, the loading noise source accounts for noise due to loading and change of loading on the body. The noise due to compressibility effects is included in the quadrupole noise source. For the current work, the quadrupole noise source is not considered, as it is a volume source that requires a grid-based flow solver.

Voutsinas and Triantos [21] previously introduced a solution of the FW-H equation into GENUVP for thickness and loading noise given by Farassat and Succi [22]. This solution discretizes the body into elements, each with associated volume and loading. Each element is a source of thickness and loading noise. Voutsinas and Triantos were successful in implementing this solution into GENUVP and validating their results against the HELINOISE and HART experiments [21].

In the current work a new acoustic formulation is added to GENUVP, based on Farassat's 1A solution of the FW-H equation [23]. The 1A formulation is a solution of the FW-H equation for thickness and loading noise by integration over the body surface. The derivation of the 1A formulation can be found in [23], therefore only the final solution is repeated in the current work:

$$4\pi p'_L(\boldsymbol{x},t) = \frac{1}{c}\int_{f=0}\left[\frac{\dot{l}_i\hat{r}_i}{r(1-M_r)^2}\right]_{ret} dS + \int_{f=0}\left[\frac{l_r - l_i M_i}{r^2(1-M_r)^2}\right]_{ret} dS + \frac{1}{c}\int_{f=0}\left[\frac{l_r(r\dot{M}_i\hat{r}_i + cM_r - cM^2)}{r^2(1-M_r)^3}\right] dS \quad (9a)$$

$$4\pi p'_T(\boldsymbol{x},t) = \\ +\frac{1}{c}\int_{f=0}\left[\frac{\rho_o v_n (r\dot{M}_i \hat{r}_i + cM_r - cM^2)}{r^2(1-M_r)^3}\right]_{ret} dS \qquad (9b)$$

$$p'(\boldsymbol{x},t) = p'_L(\boldsymbol{x},t) + p'_T(\boldsymbol{x},t) \qquad (9c)$$

where $\boldsymbol{r} = \boldsymbol{x} - \boldsymbol{y}$, $M_i = v_i/c$, $M_r = M_i r_i /r$, and $l_r = l_i r_i /r$. Equations (9a-c) give the loading (p'_L), thickness (p'_T), and total (p'), acoustic pressure at $\boldsymbol{x}$ respectively.

The loading and thickness noise terms are calculated based on aerodynamic data. As before the blades are discretized into panel elements, each of which is an acoustic source. The loading noise is calculated based on the loading and velocity of each element. Special consideration was needed for the thickness noise term since thin lifting bodies were used in the current work and the thickness noise term is dependant on v_n, the local normal velocity on the actual blade surface. To calculate v_n on the actual blade surface the velocity on the thin surface was used together with the know geometry of the airfoil section. The loading and thickness noise contributions of all elements are summed to obtain the total acoustic noise signal. It should be noted that a time shifting scheme is used in this summation process to account for the difference in travel time to the microphone for each acoustic emission.

4 GENUVP code structure

A top-level block diagram of GENUVP is shown in Figure 3. The GENUVP code has three major blocks: initialization, potential calculations, and vorticial calculations. The initialization block consists of reading input files that define the problem to be analyzed. Typical inputs include ambient conditions, geometry of the blades and other bodies, control input (collective and cyclic), rigid body motion for articulated rotors (flap and lead-lag), and desired panel density. Within the potential block the non-penetration boundary condition and the Kutta condition are satisfied. Then, output data for the current timestep can be obtained, including pressure distributions, the surrounding flowfield, and the acoustic pressure at observer positions. In the vorticial block, new wake particles are created from the near wake panel strips and the particle wake is convected downstream into position for the next set of potential calculations. The process continues until a periodic solution is obtained.

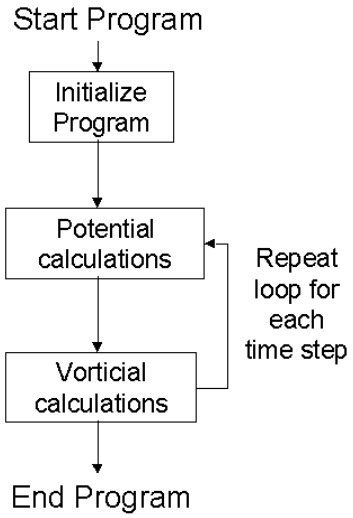

Figure 3 A top-level block diagram of GENUVP.

5 Extension to active aeroelastic analysis

Currently a great deal of research effort is being directed towards developing individual blade control (IBC) techniques for controlling rotor noise and vibration [12] [24] [25]. Essential to this research is the development of codes capable of combining advanced aerodynamic and structural dynamic models for aeroelastic modelling.

The present work is part of a collaborative project to develop a combined active aeroelastic aeroacoustic rotorcraft code. For this project GENUVP is being combined with an active structural dynamic code based on the work of Cesnik et. al. [12]. The combined code will be used for an initial evaluation of the noise reduction capability of active twist rotors. In addition, the combined code is being developed in a modular manner that will allow

studies of other individual blade control concepts [25].

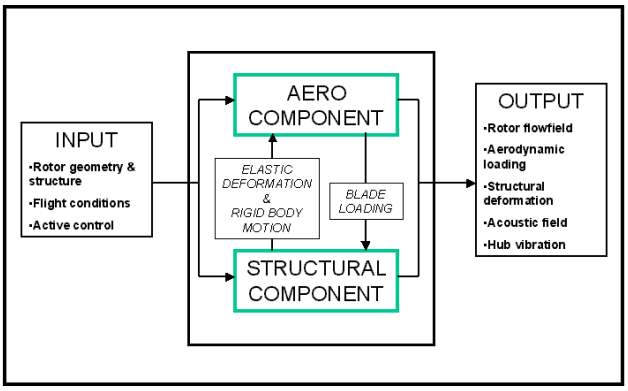

Figure 4 An overview block diagram of the combined active aeroelastic aeroacoustic rotorcraft code.

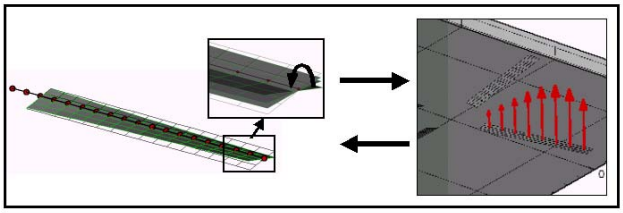

Figure 5 An illustration of the exchange of aeroelastic data between the aerodynamic and structural components.

Figure 4 gives an overview of the coupling of components to form the combined code. The combined code is a closely-coupled aeroelastic code that solves for a periodic solution in the time domain. At each timestep, aeroelastic data is exchanged between the aerodynamic component and structural component as illustrated in Figure 5. The aerodynamic component solves for an effective angle of attack at every spanwise station. Then, using 2D airfoil lookup tables aerodynamic loads are calculated and sent to the structural component. The structural component then solves for elastic deformation (displacements and rotations) and rigid body motion (flapping and lead-lagging). The elastic deformation and rate of elastic deformation are used to deform the aerodynamic mesh of the blades and alter the non-penetration boundary condition respectively. The rigid body motion is used for rigid body velocity.

6 Results and discussion

In the following section indicative aerodynamic and aeroacoustic results are presented. The results were obtained using GENUVP, without coupling to the structural component. Two configurations are considered: the ATR scale model rotor, and a UH1H scale model rotor. For both configurations only the main rotor was modelled.

6.1 ATR scale model results

Details of the ATR rotor are given in reference [12]. Some of the key modelling parameters are summarized below:

- Number of blades: 4
- Rotor type: fully articulated
- Airfoil: NACA 0012
- Radius: 1.397 m
- Pretwist: -10°, linear
- Rotor speed: 687.5 rpm

It should also be noted that the following results model the ATR operating in a heavy-gas environment (heavy gas was used during the experiment for aeroelastic scaling reasons).

Figure 6 is a visualization of the final wake geometry for the ATR in hover after 8 complete revolutions. Some upward movement of the wake particles is visible due to impulsive starting of the rotor and lack of hub modelling. Figure 7 shows a comparison of the final solution for blade spanwise loading. The comparison results are from a CAMRADII simulation, run as part of the analysis in reference [26]. One can see that there is a fairly good comparison between the two codes, with a difference in the area of the tip. This difference can be attributed to the difference in the wake geometry between the two models – i.e. the amount of wake contraction in particular as regards the explicit tip vortex shedding in the GENUVP results – as well as the lack of connecting the loading predictions in GENUVP with realistic profile data.

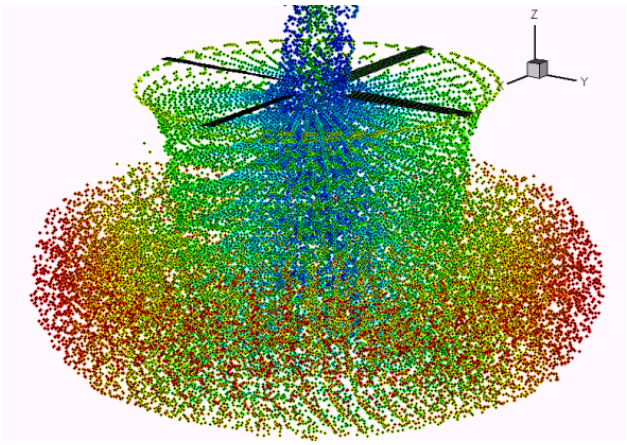

Figure 6 A visualization of the wake produced by the ATR in hover.

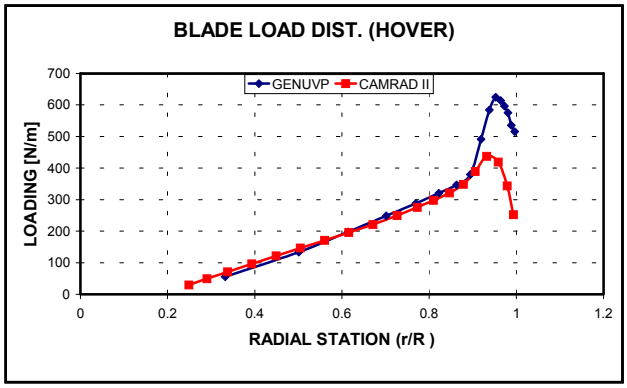

Figure 7 A comparison of blade spanwise loading for the ATR in hover.

Figure 8 shows a visualization of the wake produced by the ATR in forward flight. Figure 9 shows a comparison of the total lift loading for a single blade over a period of 2 complete revolutions of the rotor. The comparison is versus results for a finite-state induced flow model [27], done as part of the analysis in reference [26]. For this result both codes compare favourably in terms of overall trends. Differences can mainly be attributed to the difference in wake modelling, which allows GENUVP to capture higher frequency loading variation, that the finite-state induced flow model is not intended to capture [27].

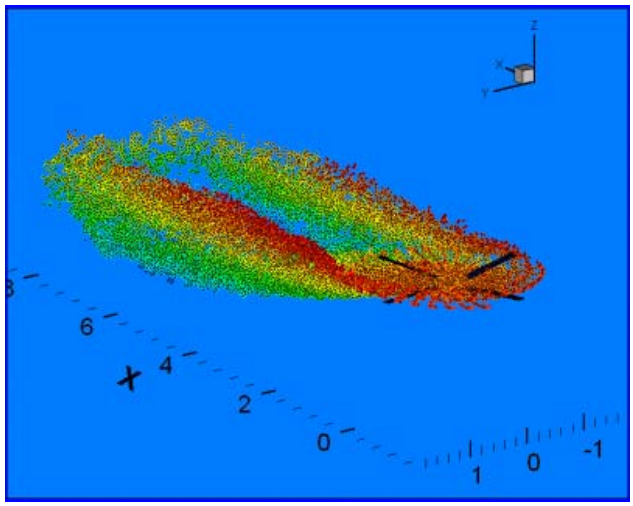

Figure 8 A visualization of the wake produced by the ATR rotor in forward flight.

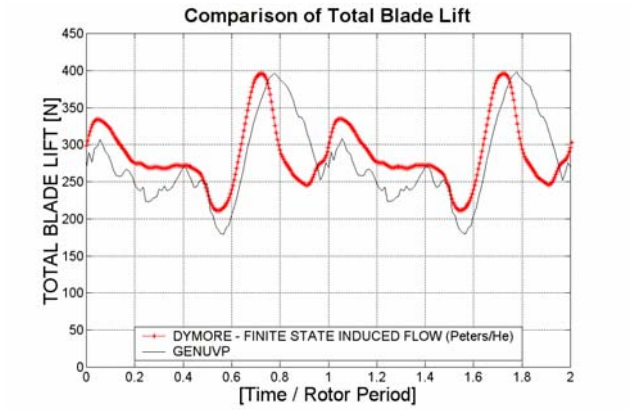

Figure 9 A comparison of total lift loading on a single blade in forward flight.

6.2 UH1H scale model results

The purpose of modeling the UH1H rotor was to validate the new acoustic formulation added to GENUVP. Details of the UH1H rotor are given in reference [28]. Some of the key modeling parameters the rotor are summarized below:

- Number of blades: 2
- Rotor type: teetering
- Airfoil: NACA 0012
- Radius: 1.829m
- Pretwist: -10.9°, linear
- Rotor speed: 1296 rpm
- Standard atmospheric conditions

Figures 10-12 show a comparison of loading, thickness, and total acoustic pressure measured at a microphone 3m from the hub, in

the plane of the rotor. Comparison results are from the original version of WOPWOP [29], which uses a slightly modified Farassat 1A acoustic formulation. The two codes agree fairly well in all three comparisons. A slight time shift is visible in the results. Also the results of the present model are reversed. This is a point to be checked.

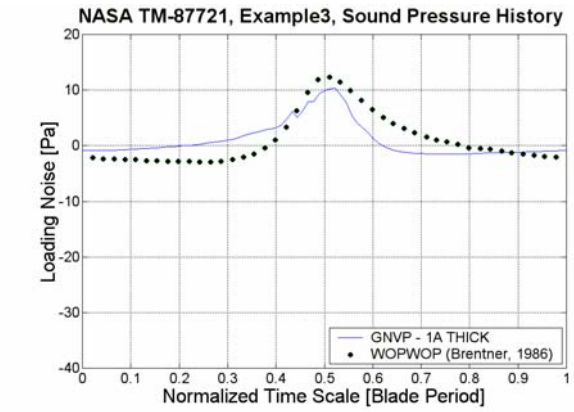

Figure 10 A comparison of loading acoustic pressure for the UH1H in hover.

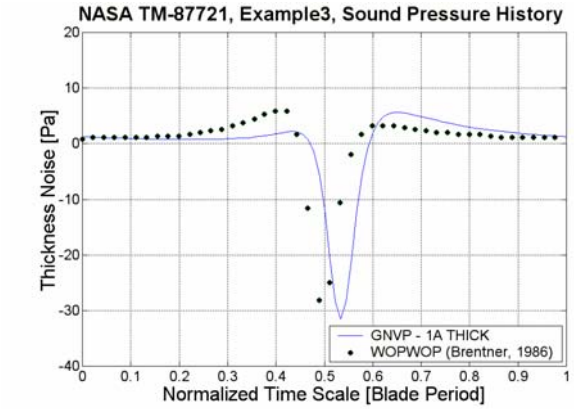

Figure 11 A comparison of thickness acoustic pressure for the UH1H in hover.

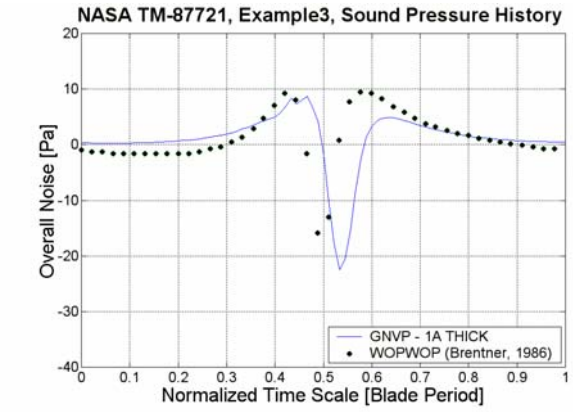

Figure 12 A comparison of total acoustic pressure for the UH1H in hover.

Figure 13 shows a visualization of the wake produced by the UH1H rotor in forward flight (μ= 0.208, 8.85° forward disc tilt) and the locations of two microphones where acoustic pressure is compared. Microphone 4 is 4m ahead of the rotor hub on the advancing side; microphone 5 is 4m ahead of the rotor hub on the retreating side. Figure 14 and Figure 15 show a comparison of total acoustic pressure at the two microphones locations. Comparison is given with both WOPWOP [29] and experimental [28] data on the advancing side, and with experimental data on the retreating side. In both cases, the overall trend is captured by GENUVP. The higher frequency component present in the experimental results is not captured by either code. While some of this high frequency component may be due to "experimental noise", it is suspected that some of the oscillation may be due to flexibility of the blades. This will be explored further using the combined aeroelastic aeroacoustic code previously mentioned. It should also be noted that compressibility effects might be present in this test case. An updated version of GENUVP [10] [11] that includes embedded Euler domains could be used to capture compressibility effects in future investigations. Figure 16 shows a comparison of sound pressure level (SPL) versus frequency for the microphone on the advancing side of the rotor. The peaks in SPL at harmonics of the blade passage frequency are accurately captured.

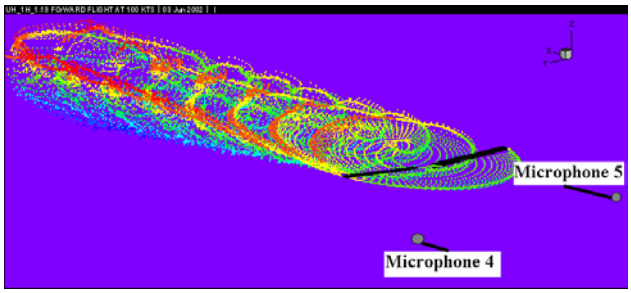

Figure 13 A visualization of the wake produced by the UH1H rotor in forward flight and microphone locations.

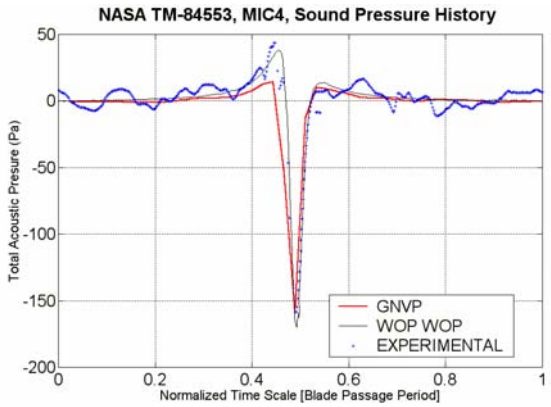

Figure 14 A comparison of total acoustic pressure (advancing side microphone) for the UH1H in forward flight.

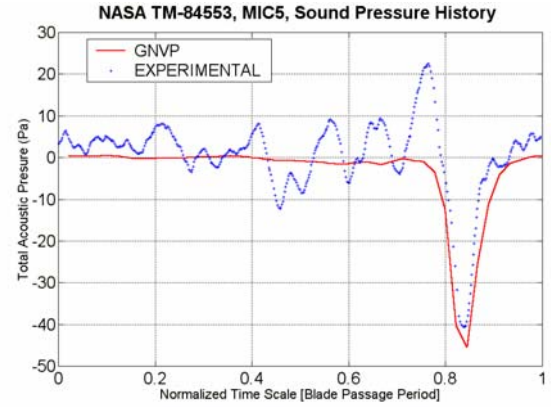

Figure 15 A comparison of total acoustic pressure (retreating side microphone) for the UH1H in forward flight.

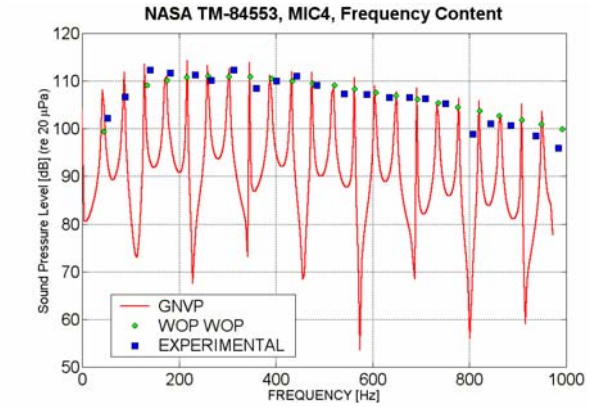

Figure 16 A comparison of frequency content of the total acoustic pressure prediction of the advancing side microphone - UH1H in forward flight.

7 Conclusions

In conclusion, the GENeral Unsteady Vortex Particle (GENUVP) has been presented. GENUVP is a panel method code coupled with a vortex particle wake for use in modelling multi-component configurations. Aerodynamic results have been presented for modelling of the ATR in hover and forward flight. Results to validate a new aeroacoustic component have been presented for hover and forward flight. This work is part of the first stage of development of a combined active aeroelastic aeroacoustic rotorcraft code that will use GENUVP as its aerodynamic component. Plans for future work include aerodynamic and aeroacoustic modelling including flexibility effects and possible use of an updated version of GENUVP, which includes embedded Euler domains.

8 Acknowledgements

This work was partially funded by the Natural Sciences and Engineering Research Council of Canada (NSERC) and the National Research Council of Canada (NRC).

9 References

[1] Strawn R.C., and Djomehri R.C., Computational modelling of hovering rotor and wake aerodynamics. *Proc. American Helicopter Society 57th Annual Forum*, Washington, DC, pp. 1723-1734, 2001.

[2] Beamier P., Chelli E., and Pahlke K., Navier-Stokes prediction of helicopter rotor performance in hover including aero-elastic effects. *Proc. American Helicopter Society 56th Annual Forum*, Virginia Beach, Virginia, pp. 391-401, 2000.

[3] Pahlke K., and Chelli E., Calculation of multibladed rotors in forward flight using 3D Navier-Stokes method. *Proc. 26th European Rotorcraft Forum,* The Hague, Netherlands, Paper No. 48, 2000.

[4] Ahmed S.R., and Vidjaja V.T., Unsteady panel method calculation of pressure distribution on BO105 model rotor blades and validation with DNW test data. *Proc. American Helicopter Society 50th Annual Forum*, Washington, DC, pp. 1211-1231, 1994.

[5] Wachspress D.A., Quackenbush T.R., and Boschitsch A.H., Rotorcraft interactional aerodynamics calculations with fast vortex/fast panel methods. *Proc. American Helicopter Society 56th Annual Forum*, Virginia Beach, Virginia, pp. 51-71, 2000.

[6] Johnson W., Rotorcraft aerodynamics models for a comprehensive analysis. *Proc. American Helicopter Society 54th Annual Forum*, Washington, DC, 1998.

[7] Leishman J.G., *Principles of Helicopter Aerodynamics*. 1st edition, Cambridge University Press, 2000.

[8] Voutsinas S.G., A GENeralized Unsteady Vortex Particle method for solving the unsteady flow around multi-component configurations. NTUA Internal Report, 1990.

[9] Voutsinas S.G., Belessis M.A., and Rados K.G., Investigation of the yawed operation of wind turbines by means of a vortex particle method. *AGARD-CP-552 FDP Symposium on Aerodynamics and Aeroacoustics of Rotorcraft*, Berlin, Germany, Paper 11, 1995.

[10] Triantos D.G., Aerodynamic and Aeroacoustic Analysis of Helicopter Rotors. *PhD dissertation*, National Technical University of Athens, Greece, 2002.

[11] Voutsinas S.G., and Triantos, D.G., High-resolution aerodynamic analysis of full helicopter configurations. *25th European Rotorcraft Forum*, Rome, Italy, Paper C11, 1999.

[12] Cesnik C.E.S., Shin S., and Wilbur M.L., Dynamic response of active twist rotor blades. *Smart Materials and Structures*, Vol. 10, No. 1, pp 62-76.

[13] Hess J.L., Calculation of potential flow about arbitrary three-dimensional lifting bodies. McDonnell Douglas Report No. MDCJ5679-01, 1972.

[14] Rehbach, C. (1973) "Calcul d'ecoulements autour d'ailes sans epaisseur avec nappes tourbillonnaires evolutives", Recherche Aerospatiale, No 2, 53-61.

[15] Beale J.T., and Majda A., High order accurate vortex methods with explicit velocity kernels. *Journal of Computational Physics*. Vol. 58, pp. 188-208, 1985.

[16] Hess J.L. and Smith A.M.O., Calculation of Non-Lifting potential flow about arbitrary three-dimensional bodies. McDonnell Douglas Rep. No ES 40622, 1968.

[17] Vassberg J.C. A fast surface panel method capable of solving million-element problems. AIAA paper 97-0168, 1997.

[18] Hockney R.W., and Eastwood J.W., *Computer Simulation Using Particles*. 1st edition, McGraw-Hill, 1981.

[19] Anderson C., A method of local corrections for computing the velocity due to a distribution of vortex blobs. *J. Comp. Physics*, Vol 62, pp 111-123, 1986.

[20] Ffowcs-Williams J.E., and Hawkings D.L., Sound generation by turbulence and surfaces in arbitrary motion. *Philosophical Transactions of the Royal Society*, A264, pp321-342, 1969.

[21] Voutsinas S.G., and Triantos D.G., Aeroacoustics of full helicopter configurations using vortex particle flow approximations. *Proc. CEAS Forum on Aeroacoustics of Rotors and Propellers*, Rome, Italy, 1999

[22] Farassat F., and Succi, G.P, A review of propeller discrete frequency noise prediction technology with emphasis on two current methods for time domain calculations. *Journal of Sound and Vibration*, Vol. 71, No. 3, pp399-419, 1980.

[23] Farassat F., and Succi G.P., The prediction of helicopter rotor discrete frequency noise. *Vertica*, Vol. 7., No. 4, pp309-320, 1983.

[24] Bernhard A.P.F., O'Neill J., Kohlhepp F., Welsh W., and Lorber P., Active Rotor Control (ARC) of a mach-scale trailing edge flap rotor. *Proc. American Helicopter Society 57th Annual Forum*, Washington, DC, pp. 1100-1127, 2001.

[25] Zimcik D., Wickramasinghe V.K., C. Yong, F. Nitzsche, 'Smart Spring' concept for active vibration control in helicopters. *Proc. American Helicopter Society 58th Annual Forum*, Montreal, Canada, 2002.

[26] Shin S, Integral twist actuation of helicopter rotor blades for vibration reduction. *PHD dissertation,* Massachusetts Institute of Technology, 2001.

[27] Peters D.A., and He C.J., Finite state induced flow models part II: three-dimensional rotor disk. *Journal of Aircraft*, Vol. 32, No. 2, pp. 323-333

[28] Conner D.A., and Hoad D.R., Reduction of high-speed impulsive noise by blade planform modification of a model helicopter rotor. NASA TM No. 84553, NASA Langley Research Center, Hampton, Virginia, 1982.

[29] Brentner K.S., Prediction of helicopter rotor discrete frequency noise – a computer program incorporating realistic blade motions and advanced acoustic formulation. NASA TM No. 87721, NASA Langley Research Center, Hampton, Virginia, 1986.